THE EFFECT OF TI AND ZR ON PRECIPITATION IN THE EXPERIMENTAL HR SERIES OF VANADIUM ALLOYS—D. T. Hoelzer, A. F. Rowcliffe, and M. Li (Oak Ridge National Laboratory)

OBJECTIVE

To investigate the effect of two processing conditions and the effectiveness of Ti and Zr solute atoms on the precipitation of interstitial C, O, and N atoms in three HR alloys using Transmission Electron Microscopy (TEM), electrical resistivity, and Vicker's hardness. The alloys that were studied had nominal compositions of V-4Cr-4Ti (HR1), V-4Cr-0.21Ti (HR6), and V-4Cr-0.37Zr (HR7).

SUMMARY

A small task was initiated to characterize the microstructure and the physical and mechanical properties of a limited number of the experimental HR vanadium alloys in order to compare with the neutron-irradiated companion specimens. The alloys examined in this study were V-4Cr-4Ti (HR1), V-4Cr-0.21Ti (HR6), and V-4Cr-0.37Zr (HR7). The effect of two thermo-mechanical processing (TMP) conditions (A and B) on precipitation of the Ti(CON) phase was studied using the HR1 alloy and the effect of Ti and Zr on the precipitation of interstitial atoms was studied using the same TMP condition (A) on HR6 and HR7. The TEM results of HR1 indicated that a low number density of non-uniformly distributed Ti(CON) precipitates having a rod-shaped morphology formed in material that was prepared using the TMP A condition (final anneal at 1000ºC/2h) while a high number density of nano-size precipitates formed in material that was prepared using the TMP B condition (final anneal at 1300ºC/2h). The Vicker's hardness was significantly higher in V-4Cr-4Ti processed by TMP B compared to TMP A. Surprisingly, the TEM analysis of HR6 and HR7 showed that Zr was much more effective in removing interstitial atoms from the matrix by precipitation than was Ti. The Vicker's hardness of the HR7 containing Zr was considerably lower than that of HR6 containing Ti.

PROGRESS AND STATUS

Background

In FY2003, twelve experimental heats of vanadium alloys designated as HR1 to HR12 were prepared at ORNL for the purpose of investigating the effects of composition, precipitation, and the presence of He on the microstructure and mechanical properties of vanadium during neutron irradiation. Details regarding the TMP conditions that were used for making the 12 HR alloys and their compositions were described previously [1]. A number of tensile (SS-J1 and SS-J2), TEM, and pre-cracked bend bar (PCBB) specimens were machined from each alloy and were inserted in the HFIR RB-17J experiment.

Experimental Procedure

In this study, a number of SS-J3 tensile and TEM specimens were machined from the remaining plate material of 7 HR alloys, which are designated as HR1, HR2, HR4, HR5, HR6, HR7, and HR10. Table 1 shows the four stages of the two TMP (A and B) conditions that were used for preparing the specimens. The specimens were machined from small plates of each alloy that were cold-rolled (except for HR2 which was warm rolled at 400ºC) to 50% reduction-in-thickness (RIT) following the third TMP stage. After the specimens were machined, they were then annealed in vacuum of ~ $1x10^{-6}$ to $1x10^{-7}$ torr at either 1000ºC/2h (TMP A) or 1300ºC/2h (TMP B).

The alloys that were investigated in this report were HR1 (V-4Cr-4Ti), HR6 (V-4Cr-0.21Ti), and HR7 (V-4Cr-0.37Zr). Table 2 shows the principle elements measured by chemical analysis of the HR1, HR6, and HR7 alloys. The HR1 alloy is the reference alloy and was prepared by arc melting material of V-4Cr-4Ti heat 832665. The HR6 and HR7 alloys were prepared by arc melting material of unalloyed V heat 820645 with 99.999% pure Cr granules and either 99.995% pure Ti slug (HR6) or 99.5% pure Zr slug (HR7).

Table 1. The four stages of the two TMP conditions that were used for preparing specimens from the HR alloys

TMP	1st Rolling Operation (stage 1)	1st HT (stage 2)	2nd Rolling Operation (stage 3)	Final HT (stage 4)
A	~50% RIT	1300ºC/1h	~50% RIT	1000ºC/2h
B	~50% RIT	1000ºC/2h	~50% RIT	1300ºC/2h

Table 2. The concentration of Cr, Ti, and Zr solute atoms and C, N, and O interstitial atoms for the HR1, HR6, and HR7 alloys

Alloy	V	Cr	Ti (wt.%)	Zr (wt.%)	C (wppm)	N (wppm)	O (wppm)
HR1	92.87	3.35	3.58	<0.002	110	100	380
HR6	95.56	4.10	0.210	<0.002	30	170	290
HR7	95.38	4.14	0.003	0.370	30	190	290

Since HR1 was prepared from a plate of V-4Cr-4Ti and HR6 and HR7 were prepared from the V ingot, the C, N, and O interstitial atoms levels were similar in HR6 and HR7 compared to HR1. The primary goal for preparing HR6 and HR7 was to study the effect of Ti or Zr (with a metal:interstitial atomic ratio of ~ 1:1) on interstitial partitioning between the matrix and precipitated phases and to evaluate the relative effectiveness of Ti and Zr as interstitial getters. The chemical analysis results indicated that the Ti:(C, O, N) ratio was ~ 1.34 in HR6 and the Zr:(C, O, N) ratio in HR7 was 1:19. Thus, there are slightly more Ti atoms relative to the interstitial atoms in HR6 than there are Zr atoms to interstitial atoms in HR7.

Results and Discussion

Property Measurements

The electrical resistivity measurements were performed on tensile specimens of HR1, HR6, and HR7 that were used in the HFIR 17J experiment and have been reported previously [2]. The Vicker's hardness was measured using the SS-J3 tensile specimens that were machined in this task. Table 3 lists the values that were reported for the electrical resistivity and for the measured Vicker's hardness of these 3 alloys. The hardness measurements are from the average of 5 indents per specimen for 2 to 4 tensile specimens using a 1000 g load.

The electrical resistivity measurements showed HR1 had a resistivity that was ~ 54 nΩ-m larger than that of HR6 and ~ 67 nΩ-m larger than that of HR7. The resistivity of the 3 HR alloys was calculated using the chemical analysis data and determining the specific resistivities for the various solute atoms in vanadium from experimentally measured values [3]. The resistivity values for some of the elements, such as Al, Zr, and Si, were assumed to be 10–15 nΩ-m/at.% based on similarities with elements having known resistivity values in vanadium. However, the total contribution of these elements to the calculated resistivity is most likely negligible and was estimated to be ~ 2 nΩ-m. Table 3 shows the calculated and measured resistivities for the HR alloys. The comparisons show good qualitative agreement between the measured and calculated resistivities for each alloy and that the larger Ti content in HR1 was primarily responsible for the significant increase in the measured resistivity over that of HR6 and HR7.

Table 3. The electrical resitivity and Vicker's hardness measured for HR1 (TMP A and B) and HR6 and HR7

Alloy	TMP	Electrical Resistivity (nΩ-m)		Vicker's Hardness
		Measured	Calculated	
HR1	A	289	282	153.4
HR1	B	-	282	186.8
HR6	A	235	225	138.7
HR7	A	223	225	94.0

The Vicker's hardness (VH) that was measured for the 3 HR alloys depended on both the TMP condition and alloy composition. In HR1, specimens prepared using TMP B showed an increase of 33.4 VH compared to those prepared using TMP A. It will be shown in the next section that the precipitation of the Ti-CON phase is altered by the higher temperature anneal used in TMP B (1300ºC) verses TMP A (1000ºC) and that this may account for the increase in hardness. The hardness that was measured in HR6 TMP A (V-4Cr-0.21Ti) was 138.7 VH, which is similar to the hardness of 139.7 VH that was measured in V-4Cr-4Ti after annealing at 1000ºC for 2h [4]. The reason for this could be due to differences in grain size and/or differences in the distribution of interstitial atoms in the vanadium matrix. The HR7 alloy had the lowest hardness value, which was 94.0 VH. This value is within the range of hardness measured for recrystallized pure vanadium [5]. This result is surprising since HR7 contains ~ 4.14 wt.% Cr (~ 4.06 at.% Cr). The Cr addition to vanadium should cause some hardening since it increases the yield and ultimate tensile strengths and decreases the ductility of vanadium [5].

Microstructural Characterization

The results of the microstructural analysis of HR1, HR6, and HR7 using transmission electron microscopy (TEM) are separated into two sections. The first section focuses on the effect of the two TMP conditions on the precipitation in HR1, which is essentially re-arc melted V-4Cr-4Ti. The second section compares the effectiveness of Ti and Zr solute atoms on precipitation in V-4Cr -X, where X = 0.21Ti (HR6) or 0.37Zr (HR7), which were prepared with the TMP A condition.

Section 1: HR1: TMP A Verses TMP B

Figure 1 shows representative bright-field TEM micrographs of the microstructures observed in HR 1 prepared by the two processing conditions. Figure 1a shows the microstructure that was observed in HR1-A (TMP A). A low number density of non-uniformly distributed Ti-CON precipitates was observed in the grains and on low angle grain boundaries. However, the microstructure was not fully recrystallized. These precipitates appear to have inhibited the recrystallization in HR1 A during annealing at 1000ºC. This result is different from past research since it has generally been found that a final annealing at 1000ºC for 2h causes full recrystallization in ~ 40% cold-rolled V-4Cr-4Ti. The HR1 alloys were 50% cold-rolled prior to the final annealing at 1000ºC for 2h. The material of HR1-B (TMP B) was annealed at 1300ºC for 2h and this resulted in full recrystallization as shown in Fig. 1b. This figure shows a grain boundary and several dislocations that were decorated with small precipitates.

The morphology of the precipitates that formed in HR1 A is shown in Fig. 2. The precipitates have shapes resembling small rods with a length-to-width aspect ratio of ~ 4–7:1. The diffraction analysis showed that the crystal structure of the precipitates was consistent with the fcc structure of the Ti(CON) phase, Fm3m space group [6]. The SAD pattern shown in Fig. 2b was obtained by tilting several degrees from the $[001]_{bcc}$ zone axis along g = 200. This imaging condition indicated that the rod-shaped Ti(CON) precipitates do not have the Baker-Nutting orientation relationship (OR) with the matrix. In previous work, it was shown that Ti(CON) precipitates with a plate-shaped morphology possess the Baker-Nutting OR with the matrix, which is $<100>_{bcc}//<110>_{fcc}$ and $\{200\}_{bcc}//\{2\bar{2}0\}_{fcc}$ [7].

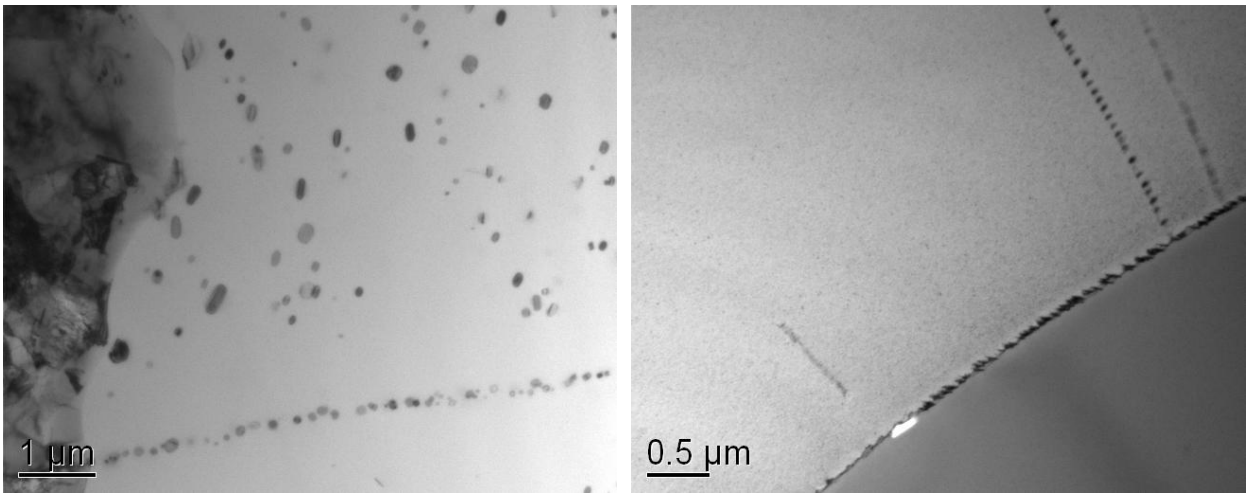

Fig. 1. Representative BF images at low magnification of the microstructures observed in HR1 prepared using (a) TMP A with a final annealing at 1000ºC/2h and (b) TMP B with a final annealing at 1300ºC/2h.

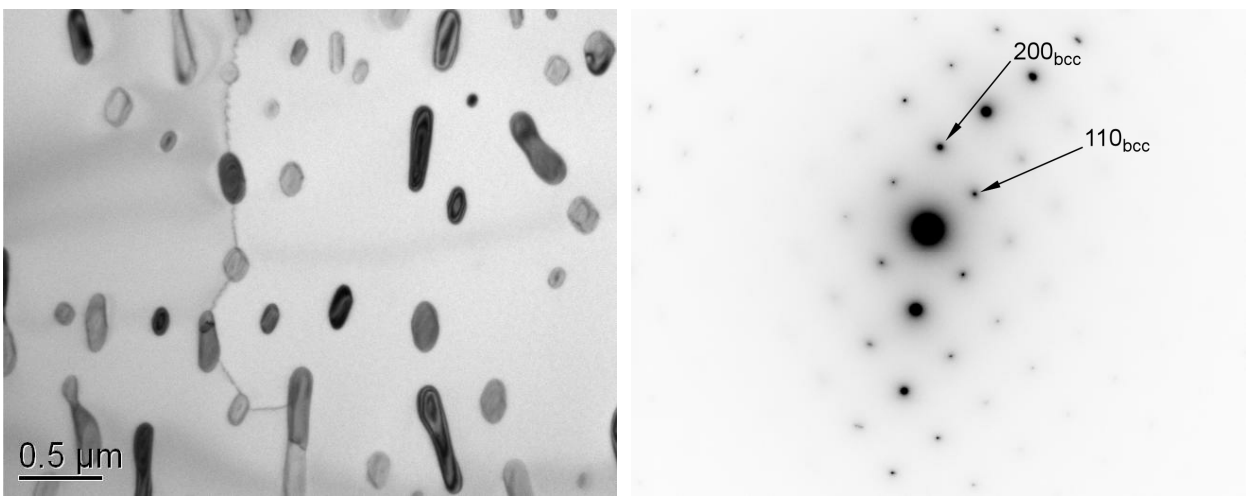

Fig. 2. The typical morphology observed for Ti(CON) precipitates in HR1 TMP A. (a) BF image showing a rod-shape morphology for the Ti(CON) phase and (b) SAD pattern tilted several degrees off B = [001] using g = 200.

The analysis of HR1-B indicated that a high number density of very small precipitates was observed in the matrix of HR1-B as shown in Fig. 3. Surprisingly, diffraction from the small precipitates was not observed at $[001]_{bcc}$ and $[011]_{bcc}$ zone axes. If these precipitates are very small plates of the Ti(CON) phase, then diffuse scattering consistent with the Baker-Nutting OR should be observed at these zone axes. However, as shown in the SAD pattern in Fig. 3b, no scattering maxima near g = ¾$(200)_{bcc}$ was observed. It has been shown that the $\{200\}_{fcc}$ reflection of the plate-shaped Ti(CON) phase will be present at the position corresponding to the $3/4\{200\}_{bcc}$ reflection. Further work involving low temperature annealing to coarsen these precipitates and allow for crystal identification is planned.

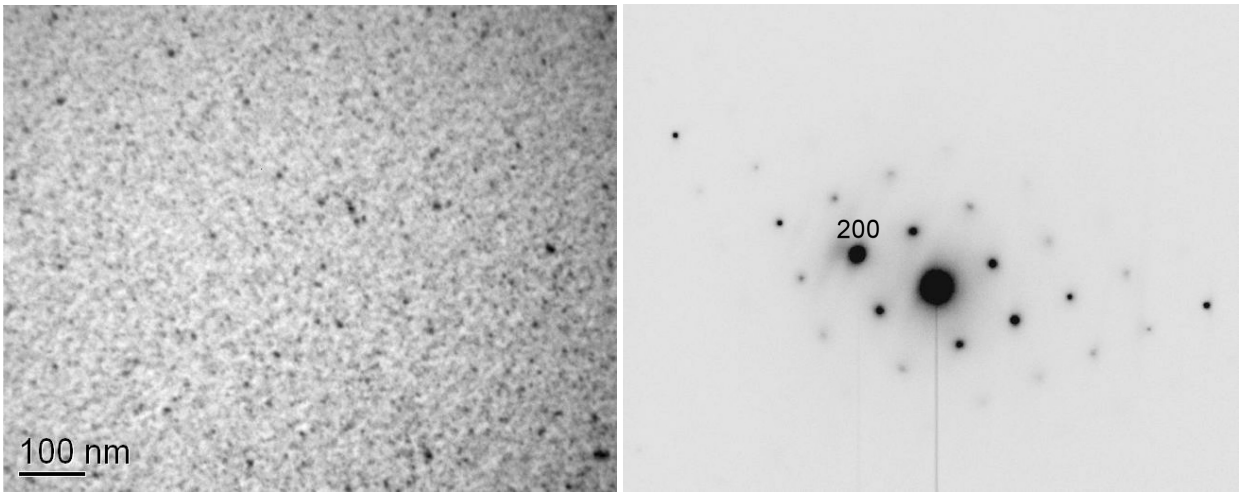

Fig. 3. A uniform distribution on nano-size Ti(CON) precipitates with a high number density was observed in the matrix of HR1 TMP B. (a) BF image recorded with g = 200 and (b) SAD pattern tilted several degrees off B = [001] using g = 200.

In addition to the small precipitates that formed in the matrix of HR1-B, larger precipitates were observed on the grain boundaries and occasionally in the matrix as shown in Fig. 4. The region shown in this figure was the only one found in the electron transparent section of the thin foil that contained the large precipitates. The long faceted side of the large precipitates was found to be parallel to the $\{100\}_{bcc}$ of the matrix. The morphology of these precipitates was determined to be like a thick plate. The SAD pattern shown in Fig. 4b was obtained from the precipitate marked with an arrow in Fig. 4a. The diffraction pattern shows the $[001]_{bcc}$ zone axis and diffraction spots from the precipitate that are consistent with the Ti(CON) phase and are close to the Baker-Nutting OR with the matrix. Close examination of the 022_{fcc} reflection showed that it was slightly rotated from the $(020)_{bcc}$ fundamental reflection indicating that a very small misorientation existed on the $\{100\}_{bcc}$ habit plane between the precipitate and matrix. In the Baker-Nutting OR, these two reflections would coincide with one another.

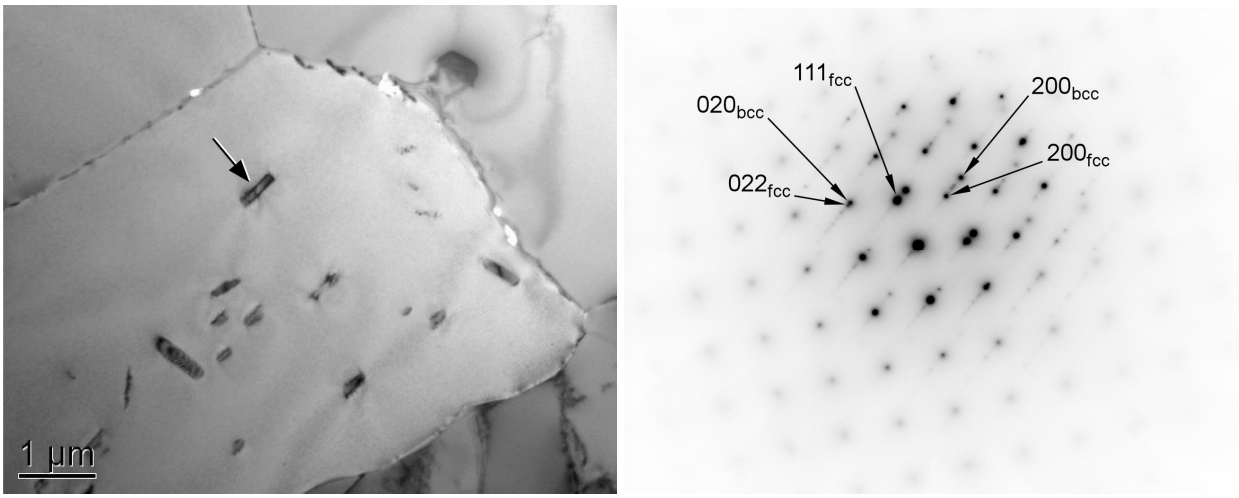

Fig. 4. A low number density of non-uniformly distributed coarse Ti(CON) precipitates was observed in HR1 TMP B. (a) BF image recorded with g = 200 near B = [001] and (b) SAD pattern of the Ti(CON) particle marked by the arrow in (a) at B = [001].

The results of this section indicate that the Ti(CON) phase formed with a rod-shape at 1000ºC and that annealing at 1300ºC caused complete, or nearly complete, dissolution, of the Ti(CON) precipitates. The high number density of nano-size precipitates that were observed in HR1 B formed during cooling from 1300ºC. The nano-size precipitates were primarily responsible for the increase in hardness of 33.4 VH that was measured in HR1 B compared to HR1 A.

It is not clear whether the low number density of thick plate Ti(CON) precipitates that were also observed in HR1 B formed during cooling or were stable at 1300ºC. It has generally been found that the Ti(CON) phase has a spherical shape at annealing temperatures above ~ 1000ºC in order to minimize the interfacial area to volume ratio with the matrix. Below ~ 1000ºC, a plate shape is preferred since the larger interfacial area is compensated by the low interfacial energy of $\{100\}_{bcc}$ habit plane. Thus, it seems more likely that the thick plate Ti(CON) phase nucleated heterogeneously within the matrix and on grain boundaries during cooling. However, the defect in the matrix that was responsible for the heterogeneous nucleation of the thick plate Ti(CON) phase is not known. Experiments utilizing rapid cooling rates are required in order to resolve the question of whether the Ti(CON) phase is fully or partially dissolved at 1300ºC. The results of this experiment would also answer the uncertainty of whether the thick plate Ti(CON) phase was stable at 1300ºC or formed during cooling from the annealing temperature.

Section 2: HR6 and HR7 (Both TMP A)

The TEM analysis of HR6 and HR7 showed significant differences in the effectiveness of Ti (HR6) and Zr (HR7) on removing interstitial atoms from the matrix by precipitation. Figure 5 shows low magnification micrographs of the microstructures that were observed in these alloys. Very few precipitates were observed in the matrix of HR6 (Fig. 5a). However, a large number density of precipitates with a bimodal size distribution was observed in the matrix of HR7 (Fig. 5b). Another difference that was observed between these two alloys was the degree of recrystallization. HR6 contained a fully recrystallized microstructure while HR7 contained a partially recrystallized microstructure with some regions consisting of dislocation substructures as seen in the lower right corner of Fig. 5b.

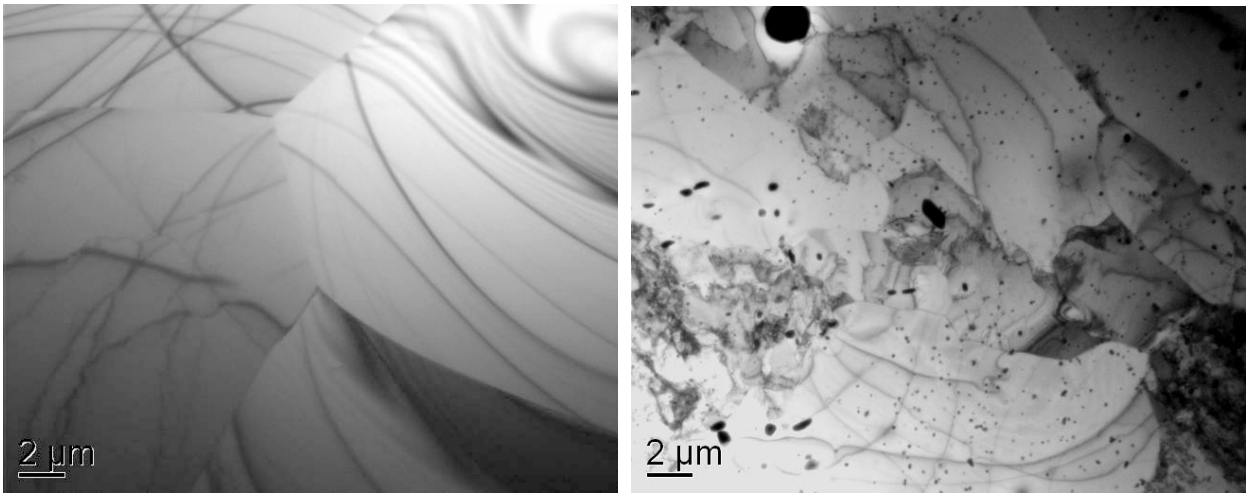

Fig. 5. Representative BF images at low magnification of the microstructures observed in (a) HR6 and (b) HR7. Both alloys were prepared using the TMP A condition which had a final annealing at 1000ºC/2h.

Figure 6 shows a stinger of precipitates that were observed in HR6. These precipitates had a spherical shape and were ~ 0.1 μm in size. The preliminary study of their crystal structure has shown that it is not consistent with the fcc crystal structure of the Ti(CON) phase. The SAD pattern shown in Fig. 6b shows extra diffraction spots from a precipitate observed in the matrix near the $[011]_{bcc}$ zone axis. This pattern contains a systematic row of reflections from the precipitate that are double diffracted by the matrix fundamental reflections (dashed lines). The d-spacing that was determined from the reflections was found to be ~ 0.289 nm. This d-spacing value was not consistent with the fcc Ti(CON) phase, which has a lattice parameter of a=~0.42 nm. It also did not correlate with the anatase TiO_2 phase, $I4_1/amd$ space group with a = 0.378 nm and c = 0.951 nm. Further diffraction analysis to identify this phase is planned.

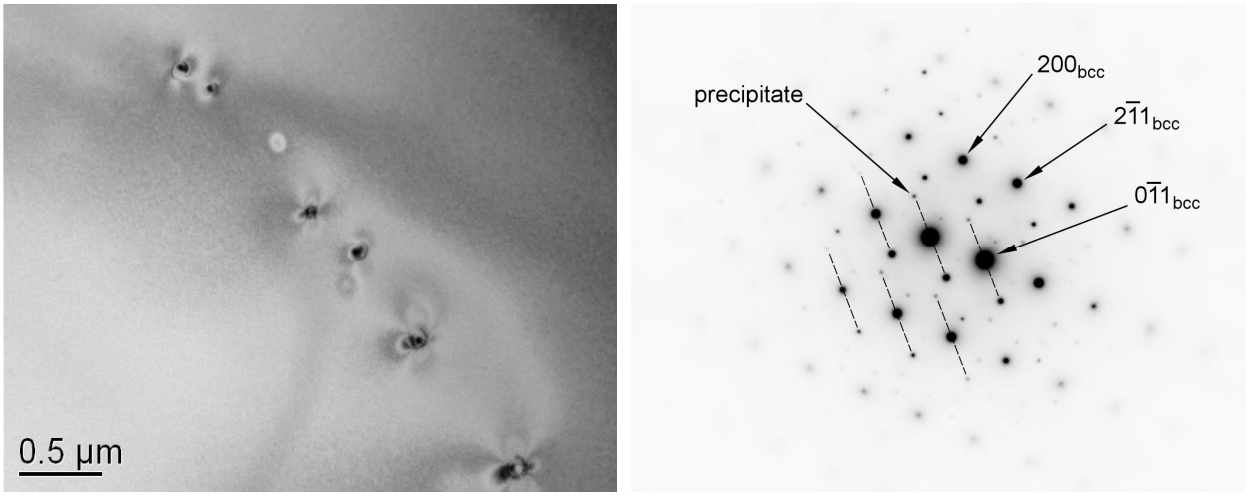

Fig 6. A very low number density of precipitates was observed in the matrix of HR1. (a) BF image of a stringer of precipitates and (b) SAD pattern of the matrix containing one precipitate at B = [011].

Figure 7 shows the bimodal size distribution of precipitates that were observed in different areas of the microstructure of HR7. The size range of the smaller precipitates was 15 to ~ 50 nm while that of the larger precipitates was 0.1 to 0.3 μm. The precipitates were distributed non-uniformly in the matrix of both unrecrystallized (Fig. 7b) and recrystallized (Fig. 7b) regions of the microstructure. The resistance of HR7 to recrystallization was due to the presence of these precipitates.

The composition and structure of the precipitates observed in HR7 were analyzed by x-ray energy dispersive spectroscopy (XEDS) and electron diffraction, respectively. The XEDS analysis indicated that both the small and large precipitates were Zr-rich. An oxygen peak was identified in the spectra of the large precipitates. However, it was not possible to observe oxygen in the XEDS spectra of the smaller precipitates due to background noise. Figure 8 shows a large Zr-rich precipitate that was analyzed by SAD. Internal planar defects that were identified as twins were observed in the precipitate (Fig. 8a). The SAD pattern shown in Fig. 8b was indexed and found to be consistent with the $0\bar{1}1$ zone axis of ZrO_2 based on the monoclinic crystal structure with $P2_1/c$ space group. This zone axis also shows the twin relationship observed in the precipitate. The twin variants are labeled as T_1 and T_2 with the T_2 variant showing less intense reflections owing to the smaller volume fraction in the precipitate. The twin plane for both variants is (100), which is consistent with published results [8]. Further work is necessary to determine the phase of the smaller precipitates.

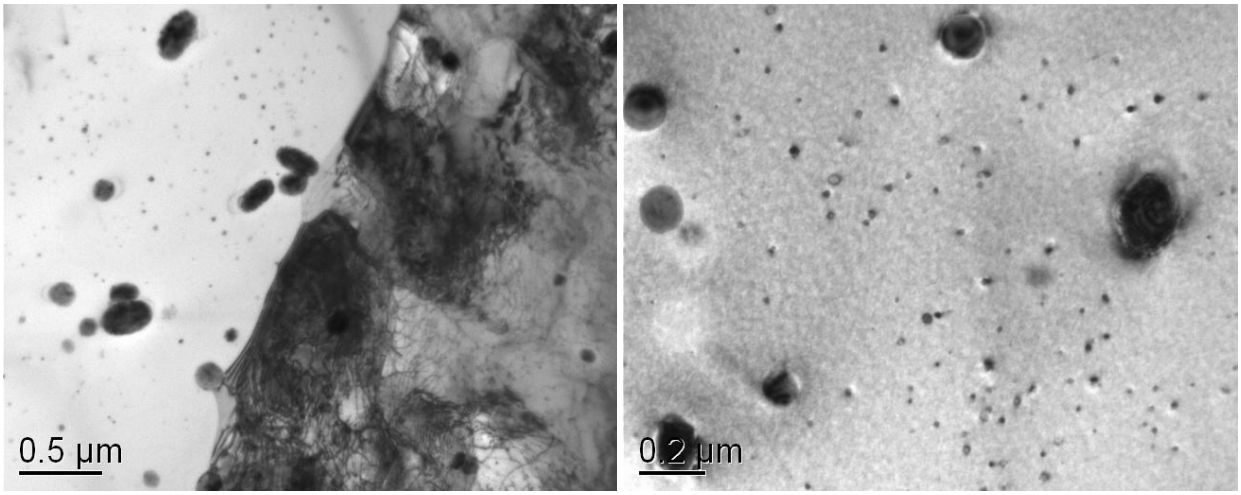

Fig. 7. (a) BF image showing a bimodal distribution of Zr-rich precipitates near a grain boundary that separates a recrystallized grain (left) and unrecrystallized grain (right) in HR7. (b) BF image showing the two precipitate sizes in the matrix of HR7 at higher magnification.

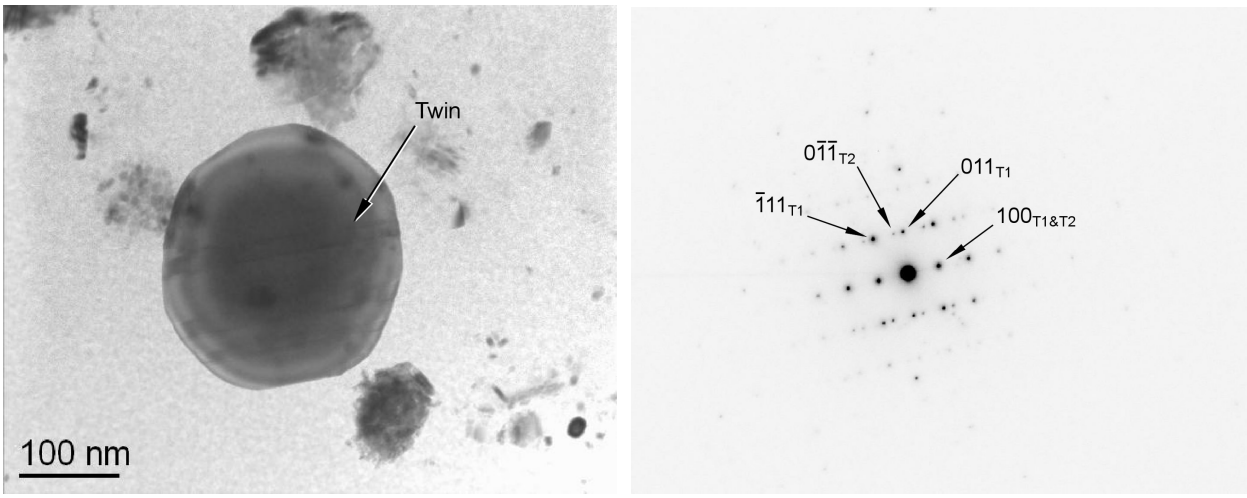

Fig. 8. Structural analysis of the large Zr-rich precipitates. (a) BF image showing twins in the precipitate and (b) SAD pattern of the twin relationship that is consistent with the $0\bar{1}1$ zone axis of ZrO_2 and (100) twin plane.

Several questions arise based on the results above that showed the larger precipitates to be ZrO_2. This oxide phase should be very stable at high temperatures. It is possible that the large ZrO_2 precipitates formed during the first annealing at 1300ºC in stage 2 (see Table 1). The diffusivity of Zr and the interstitial atoms should be very high at this temperature and this would lead to both a low nucleation rate and high growth rate for precipitates. The second annealing for HR7 was at 1000ºC in stage 4. A decrease in the solubility range of the interstitial atoms at 1000ºC would favor additional nucleation of precipitates. The smaller size may be attributed to lower diffusion rates at 1000ºC. Another issue that needed to be resolved is whether the ZrO_2 precipitates contain any significant levels of N and C. The C content of HR7 was only ~ 30 wppm, but the N content was ~ 190 wppm. If ZrO_2 phase has a low solubility range for C and N, then the smaller Zr-rich precipitates may be a different phase, such as

Zr(CN). The crystal structures for ZrC and ZrN are the same and are similar to that of the fcc Ti(CON) phase, which means that C and N would be isomorphous in the structure. Further work is required to determine the stability of ZrO_2 at 1300ºC and the interstitial content of the smaller precipitates. It will be necessary to apply electron energy loss spectroscopy (EELS) to determine the interstitial content of the smaller precipitates.

As described in the experimental procedures, HR6 and HR7 were prepared with Ti and Zr additions, respectively, that were closely matched on a 1:1 atomic percent ratio with the total concentration of interstitial C, O, and N atoms. The results indicate that Zr is much more effective in removing interstitial atoms from the matrix by precipitation than Ti. Both the hardness and electrical resistivity data support this conclusion. HR6 had a higher hardness than HR7 (138.7 VH vs. 94.0 VH) and a higher electrical resistivity (235 nΩ-m vs. 223 nΩ-m). These results are consistent with a large fraction of interstitial and solute Ti atoms in solution in HR6. On the other hand, the solute Zr atoms in HR7 react with the interstitial atoms and remove them from solution, which lowers the hardness and electrical resistivity. What is surprising is that the precipitates observed in HR7 do not cause any strengthening since the hardness value that was measured is within the range of hardness that is typically measured in unalloyed recrystallized vanadium.

Conclusions

The results of the characterization of three experimental HR vanadium alloys (HR1: V-4Cr-4Ti, HR6: V-4Cr-0.21Ti, and HR7: V-4Cr-0.37Zr) using TEM, electrical resistivity, and microhardness has revealed the following:

(1) In HR1, the final anneal at 1300ºC (TMP B) caused complete, or nearly complete, dissolution of the coarse Ti(CON) precipitates that formed during annealing at 1000ºC (TMP A). This resulted in the formation of a high number density of nano-size precipitates, presumed to be the Ti(CON) phase, in HR1 B compared to the low number density of non-uniformly distributed Ti(CON) precipitates having a rod-shaped morphology that formed in HR1 A.

(2) Significant hardening occurred in HR1 B due to the high-number density of nano-size precipitates. The Vicker's hardness increased from 153.4 in HR1 A to 186.8 in HR1 B.

(3) The presence of 0.37wt.%Zr in HR7 A (V-4Cr-0.37Zr) was found to be much more effective in removing interstitial atoms from the matrix by precipitation than the presence of 0.21wt.%Ti in HR6 A (V-4Cr-0.21Ti). Notably, precipitates having a bimodal size distribution formed in HR7 A. The large precipitates were identified as monoclinic ZrO_2 phase while the smaller precipitates were Zr-rich but were not identified.

(4) The Vicker's hardness and electrical resistivity measured in HR7 A were lower than that measured in HR6 A. These results indicated that a larger fraction of interstitial atoms were removed from the matrix in HR7 A compared to HR6 and this could be attributed to the Zr addition.

Future Work

If resources permit, the characterization of other HR alloys will be conducted. In addition, tensile tests are also planned for investigating the effects of composition and microstructural differences on the tensile properties and dynamic strain aging (DSA) behavior of the HR alloys.

References

[1] D. T. Hoelzer, A. F. Rowcliffe, and L. T. Gibson, DOE/ER-0313/34 (2003) 22–26.
[2] M. Li, D. T. Hoelzer, and S. J. Zinkle, DOE/ER-0313/34 (2003) 2–5.
[3] S. J. Zinkle, A. N. Gubbi, and W. S. Eatherly, DOE/ER-0313/21 (1996) 15–19.
[4] D. T. Hoelzer, M. K. West, S. J. Zinkle, and A. F. Rowcliffe, J. Nucl. Mater. 283–287 (2000) 616–621.

[5] D. L. Harrod and R. E. Gold, Int. Metals Reviews 25(4) (1980) 163–221.
[6] D. T. Hoelzer, DOE/ER-0313/25 (1998) 59–63.
[7] D. T. Hoelzer and S. J. Zinkle, DOE/ER-0313/29 (2000) 19–25.
[8] M. Ruhle and A. H. Heuer, in N. Claussen, M. Ruhle, and A. H. Heuer (ed.), Advances in Ceramics, Vol. 12 (The American Ceramic Society, Columbus, OH, 1983) 14–32.